# Faraday waves on nematic liquid crystals: Effect of Marangoni flow and thermal phase transition

M. Hernández-Contreras*

*Departamento de Física, Centro de Investigación y Estudios Avanzados del Instituto Politécnico Nacional*
*Apartado Postal 14-740, México Distrito Federal, Mexico*

(Received 2 August 2013; revised manuscript received 4 October 2013; published 23 December 2013)

The parametric instability in nematic liquid crystal layers has been studied using linear stability theory. Using material parameters of typical nematics, the neutral stability curve and dispersion relation of a system that presents critical subharmonic waves is obtained. The critical acceleration and wave number of the unstable stationary waves are discontinuous at the nematic-isotropic transition temperature and conform to similar sharp changes experienced by the viscosities and surface tension as a function of temperature. Due to Marangoni flow the curve of the critical acceleration as a function of excitation frequency exhibits a minimum. If the Marangoni flow is neglected and the dynamical viscosity is increased, a monotonously increasing dependence of the acceleration in terms of oscillation frequency is observed. A bicritical instability is reached for a layer thickness of a few millimeters. A well-defined subharmonic wave is attained when the thickness of the layer is further increased. The dispersion relation of these waves displays a discontinuous shift at high frequencies due to alternating secondary thresholds of Faraday waves. At negligible external forcing we determined the dispersion relationship of thermal surface waves.

DOI: 10.1103/PhysRevE.88.062311 PACS number(s): 82.70.−y, 83.80.Xz, 61.30.Dk, 68.03.−g

## I. INTRODUCTION

The Faraday instability due to the vertical motion of a vessel containing a liquid is used in experimental systems for studying nonequilibrium dynamics in complex fluids [1–8]. At the onset of the instability, the formation of patterns on the liquid surface can be made functional with potential technological application in electro-optical devices once the underlying dynamical mechanism of these structural formations is clearly understood and controlled. To date, most studies have been performed on Newtonian liquids [9–12], ferrofluids [13–15], polymeric [16–19], and wormlike micellar [20,21] solutions. Typically the polymeric and micellar solutions are formed by several chemical species. Consequently, current research efforts have allowed us to understand how their multicomponent nature affects their viscoelastic behavior and development of hysteretic high amplitude waves as was demonstrated in wormlike micelles [21]. In contrast, much less is known about this parametric instability in complex fluids that are anisotropic, such as liquid crystals. In a recent paper, Ballesta *et al*. [22] presented birefringence measurements in suspensions of rodlike *fd* viruses. In this paper [22], the authors experimentally studied the parametric instability on lyotropic liquid crystals and demonstrated a phase change from isotropic to local nematic ordering of the nematogens at the surface wave's crest as was detected with cross-polarizers. This phase change induced by a hydrodynamic instability originates due to variations of the viscosity of the liquid in a sublayer near the surface where viscosity changes were produced by the associated shear flow of the Faraday wave. In this study, we investigate the effect of the hydrodynamic coupling between the fluid velocity and collective orientational director, as well as the temperature-induced phase change and the effect of Marangoni flow, on the Faraday wave in liquid crystals. The observed onset of Faraday waves has being successfully described by linear stability theory [9]. This approach reproduces the experimental dispersion relation of Newtonian liquids [11], and its validity has also been confirmed through experiments [3,18] and computer simulations on viscous fluids [23]. In the present paper we used this linear stability approach to study the parametric instability onset in nematic liquids for pure nematogens (thermotropic liquid crystals). We analyzed two model systems that were subjected to a vertical temperature gradient under the action of an externally applied static magnetic field that was parallel to the equilibrium planar interface. The field fixes the orientation of the nematic director either parallel or perpendicular to the velocity wave vector. In the first case, hydrodynamic coupling occurs between the director and the velocity field. In the second case, there can be no such coupling. We determined the dynamical properties such as the stability curves and dispersion relationships of the Faraday waves of the systems. We present results for realizable nematic liquid with a depth of millimeters and within the typical frequency of oscillations of present experimental techniques. Furthermore, linear stability analysis for the critical acceleration and wave number at instability onset indicates that both parameters exhibit discontinuous behavior at the nematic-isotropic transition temperature in accordance with similar sharp jumps displayed by viscosities and surface tension due to Marangoni flow as a function of this thermodynamic variable. In Sec. II the boundary conditions of a nematic liquid under a magnetic field that is collinear with the wave vector and their use in deriving the surface mode is presented. We present here our main result for the prediction of the critical acceleration and wave number as a function of temperature of the nematic liquid that undergo a nematic-isotropic transition and of the effect of Marangoni flow. The dispersion relation driven by thermal fluctuations, and a numerical analysis of the surface mode of a model nematic liquid layer with high viscosities are presented. In Sec. III we consider a model system in which the external magnetic field is perpendicular to the wave vector, and, therefore, the nematic director is decoupled from the

*marther@fis.cinvestav.mx

 

flux. Consequently, a recursive relation results yielding the parametric surface modes corresponding to an isotropic fluid; these results were used in Sec. II to determine the isotropic side of the critical dispersion relation as a function of temperature. Section IV presents a summary of our main results.

## II. HORIZONTAL MAGNETIC FIELD PARALLEL TO THE WAVE VECTOR ORIENTED ALONG THE *X* AXIS

We consider a nematic liquid layer of average depth $L$ and infinite lateral extension subjected to vertical acceleration $g(t) = g - a\cos(\omega t)$, where $g$ is the gravitational acceleration in a reference frame moving with the container, $a$ is the external driving acceleration, and the frequency of oscillation is denoted by $\omega$. A static external magnetic field $\mathbf{H} = \mathbf{B}\mu_0^{-1}$ orients the director $\mathbf{n}$ of the nematogens in the $x$ axis direction and parallel to the liquid-air interface. $\mu_0 = 4\pi \times 10^{-7}$ N/A$^2$ is the permeability of free space, and $\mathbf{B}$ is the magnetic induction. We assume the equilibrium interface is located at $z = 0$ and that the bulk of the system occupies the space $-L \leqslant z \leqslant 0$. The system is symmetric in the spatial coordinates $x$ and $y$. Thus, we may assume the generated surface wave propagates in the $x$ direction with wave vector $\mathbf{k}$. Langevin [24] calculated that for a quiescent fluid thermal fluctuations produce bulk undulations of the nematic layers due to elastic variations of the director $\mathbf{n}$. The frequencies of the elastic distortion of the director field are on the order of $\omega_{\text{undulation}} = (Kk^2 + \chi_a \mathbf{H}\cdot\mathbf{H})/\eta = 9.9$ Hz (where $K = 10^{-11}$ N is the splay module, $k = 3 \times 10^4$ m$^{-1}$ is the wave number of the thermal wave, the anisotropic magnetic susceptibility in SI units is $\chi_a = 4\pi \times 10^{-7}$, which is defined as the difference between the parallel and perpendicular components of the magnetic susceptibility tensor with respect to the director [25,26], the magnetic induction of strength $|\mathbf{B}| = 0.3$ T, and the mean viscosity $\eta = 0.01$ Pa s), which are much less than both the frequencies of external excitation $w$ and the frequency associated with inertial effects $\omega_{\text{inertia}}/\omega_{\text{undulation}} = 10^6$ (where $\omega_{\text{inertia}} = \eta/\rho L^2$, for MBBA density $\rho = 1000$ kg/m$^3$ and layer thickness $L = 4.5$ mm). Therefore we neglect its variation dynamics in the governing hydrodynamic equations of the surface wave [24,27]. We will not consider the damping effect due to viscous boundary layers produced by the walls of the vessel and beneath the surface. Thus, the equation of motion for the velocity field, referenced to the moving frame, describes a liquid with surface tension $\gamma$ (the surface tension is taken to be a scalar quantity because experiments indicate that this parameter is isotropic in nematic liquids [28], as demonstrated in Fig. 2 below), shear viscosities $\eta_2$, $\eta_3$ and $\eta'$ [25,29], and viscous stress tensor [24,27]

$$\boldsymbol{\sigma}'_{ij} = \eta' \mathbf{n}_i \mathbf{n}_j \mathbf{V}_{lo} \mathbf{n}_l \mathbf{n}_o + 2\eta_2 \mathbf{V}_{ij} + 2(\eta_3 - \eta_2)(\mathbf{n}_i \mathbf{n}_l \mathbf{V}_{lj} + \mathbf{n}_j \mathbf{n}_l \mathbf{V}_{li}). \quad (1)$$

The viscosities are defined in terms of the Leslie viscosity coefficients $\alpha_i$, $i = 1,\ldots,5$ through $\eta_3 = (\alpha_4 + \alpha_5)/2 - \alpha_2\gamma_2/(2\gamma_1)$, $\eta_2 = \alpha_4/2$, $\eta' = \alpha_1 + \gamma_2^2/\gamma_1$, where $\gamma_1 = \alpha_3 - \alpha_2$, and $\gamma_2 = \alpha_3 + \alpha_2$ [24]. In Eq. (1) the unit vector director of the nematic molecules is represented by $\mathbf{n} = (1,0,0)$. $\mathbf{V}_{ij} = (\partial_i v_j + \partial_j v_i)/2$ is the second rank velocity tensor with components $i,j,l,o = x,y,z$. The velocity satisfies the linearized Navier-Stokes equation [24]:

$$\rho \frac{\partial \mathbf{v}}{\partial t} = \boldsymbol{\nabla}\cdot\boldsymbol{\sigma}, \quad (2)$$

where $\boldsymbol{\sigma} = -p\mathbf{I} + \boldsymbol{\sigma}' + \boldsymbol{\sigma}^r - \rho g(t)\hat{\mathbf{e}}_z\hat{\mathbf{e}}_z$, with $\hat{\mathbf{e}}_z$ being a unit vector along the $z$ axis and $(\mathbf{I})_{\beta,\delta} = 1$ if $\beta = \delta$ and 0 otherwise. $p$ is the hydrostatic fluid pressure, and $\rho$ is the density. The elastic deformation of the interface is governed by the surface tension through the stress tensor $\sigma^r$, which components in the boundary conditions are provided below.

Because the liquid is maintained under a constant vertical temperature gradient that produces a Marangoni instability [30], the temperature variations in the liquid are described by the linearized heat diffusion equation:

$$\partial_t T = A v_z + \alpha\left(\partial_z^2 T + \partial_x^2 T\right), \quad (3)$$

where $T$ is the local temperature whose vertical gradient per unit length $A$ is fixed in the experimental setup and taken to be $A = -3\,^\circ$C/mm [28]. This value is taken to be negative for heating from the air side [30]. $\alpha$ is the thermal diffusivity. For frequencies much less than the first sound frequency of the liquid, the incompressibility condition holds:

$$\boldsymbol{\nabla}\cdot\mathbf{v} = 0. \quad (4)$$

At the interface $z = 0$, the boundary conditions are given by the normal and shear stresses which satisfy the balance equations:

$$\sigma_{zz} = 0, \quad \sigma_{xz} = 0, \quad \sigma_{yz} = 0. \quad (5)$$

However, the normal restoring force is given by the Laplace expression due to the mean surface tension at the equilibrium temperature [30] and has the following form:

$$\sigma^r_{zz} = f_z = \gamma\left(\partial_x^2 + \partial_y^2\right)\zeta(x). \quad (6)$$

$\zeta$ is the normal displacement of the interface from its equilibrium position, and the tangential forces are the following [30]:

$$\sigma^r_{xz} = f_x = \frac{d\gamma}{dT}[\partial_x T - A\partial_x \zeta(x)], \quad \sigma^r_{yz} = 0. \quad (7)$$

$\sigma^r_{xz}$ takes into account Marangoni flow due only to the variation of the surface tension with temperature. Notice that we have neglected the contributions arising from tangential shear and dilational surface viscosities [31], which are important for surface-active interfaces [32] or for surfaces with adsorbed molecules as occurs in foams or emulsions [33], because these surface dilational properties have not been measured for MMBA nematics. Because the displacement $\zeta$ is small compared with the wavelength, the kinematic condition can be written as follows:

$$\partial_t \zeta = v_z, \quad \text{at} \quad z = 0, \quad \kappa\partial_z T = 0, \quad (8)$$

where the last equality considers a thermally insulated surface with fixed flux [30,31], and $\kappa$ is the thermal conductivity. At the bottom of the container ($z = -L$), the no-slip

$$\mathbf{v} = \mathbf{0} \quad (9)$$

and no-penetration

$$\partial_z v_z = 0 \quad (10)$$

boundary condition applies, together with $T = 0$ °C at the bottom solid wall [31].

The first two conditions of Eq. (5) can be written in terms of a single expression containing the normal velocity component

$$\eta_3\left[\nabla_\perp^2 - \partial_z^2\right]v_z = \frac{d\gamma}{dT}\partial_x^2[T - A\zeta(x)] \tag{11}$$

using Eq. (7).

We demonstrated in Ref. [34] that by taking the divergence $\nabla_\perp := (\partial_x, \partial_y)$ of (2), an equation for the pressure is attained which when combined with the expression that results from applying the Fourier transform $\widetilde{u} = \int d^2r e^{i\mathbf{k}\cdot\mathbf{r}}u$, with $i = \sqrt{-1}$, to the double curl of the $z$ component of Eq. (2) it yields the following boundary conditions at $z = 0$:

$$\begin{aligned}&\left[\partial_t + (\nu_3 + 2\nu_2)k^2 - \nu_2\partial_z^2\right]\partial_z\widetilde{v}_z \\ &\quad = -(\nu_3 - \nu_2)\left[-2ik^3 + ik\partial_z^2\right]\widetilde{v}_x + \nu' ik^3\widetilde{v}_x \\ &\qquad - g(t)k^2\widetilde{\zeta} - \frac{\gamma}{\rho}k^4\widetilde{\zeta},\end{aligned} \tag{12}$$

and from Eq. (11),

$$\nu_3\left[k^2 + \partial_z^2\right]\widetilde{v}_z = \frac{k^2}{\rho}\frac{d\gamma}{dT}[\widetilde{T} - A\widetilde{\zeta}(x)]; \tag{13}$$

and from the second identity of Eqs. (7) and (8)–(9) we obtain

$$\begin{aligned}&\left[\partial_t - \nu_2\left(\partial_z^2 - k^2\right)\right]\left(\partial_z^2 - k^2\right)\widetilde{v}_z \\ &\quad = (\nu_3 - \nu_2)\left(-\partial_z^2 + k^2\right)[ik\partial_z\widetilde{v}_x + k^2\widetilde{v}_z] + \nu' ik^3\partial_z\widetilde{v}_x,\end{aligned} \tag{14}$$

where $\nu_j = \eta_j/\rho$, $j = 2,3$, $\nu' = \eta'/\rho$.

Additionally for all $z$ the heat diffusion equation is valid:

$$\partial_t\widetilde{T} = A\widetilde{v}_z + \alpha\left(\partial_z^2\widetilde{T} - k^2\widetilde{T}\right), \tag{15}$$

which was not considered in our previous work [34] and led to a different dispersion relation below. Because $g(t)$ is a periodic function with period $2\pi/w$, the Floquet theory renders solutions to Eqs. (4) and (12)–(15) as superpositions of the time-periodic functions [9,11]:

$$\widetilde{\zeta}(t) = \sum_{n=-\infty}^{\infty}\widetilde{\zeta}_n e^{\mu_n t}, \tag{16}$$

with $\mu_n(w) = s + i(n + \alpha_r)w$. $s$ and $\alpha_r$ are real valued [9]. The harmonic surface wave (Har) is characterized by $\alpha_r = 0$,and the subharmonic wave's (Sub) response is characterized by $\alpha_r = 1/2$. Due to the reality condition on the above mentioned displacement field, $\widetilde{\zeta}_n = \widetilde{\zeta}_n^*$, with $\alpha_r = 0$ and $\widetilde{\zeta}_n = \widetilde{\zeta}_{n-1}^*$ for $\alpha_r = 1/2$. A similar expansion holds for the velocity $\widetilde{v}_z := \widetilde{w}(z,t)$:

$$\widetilde{w}(z,t) = \sum_{n=-\infty}^{\infty}\widetilde{w}_n(z)e^{\mu_n t}, \tag{17}$$

which, when substituted in Eqs. (4) and (14), yields

$$\left[\partial_z^4 + b_n\partial_z^2 + c_n\right]\widetilde{w}_n(z) = 0, \tag{18}$$

where $\partial_z^k$, is the $k$th derivative with respect to $z$, and the coefficients are as follows:

$$b_n = -\left[\frac{\mu_n}{\nu_3} + k^2\left(2 + \frac{\nu'}{\nu_3}\right)\right], \quad c_n = k^2\left[\frac{\mu_n}{\nu_3} + k^2\right]. \tag{19}$$

The solutions of Eq. (18) are of the form $\widetilde{w}_n(z) \sim e^{m(k)z}$. Therefore, making the change of variable $V = m^2$ yields the following quadratic equation:

$$V^2 + b_n V + c_n = 0. \tag{20}$$

We numerically calculated the two main modes $V_j = m_j^2$, $j = 1,2$.

Thus, the total solution of Eq. (18) can be written as follows:

$$\begin{aligned}\widetilde{w}_n(z) = {}& P_n\cosh(zm_1) + Q_n\sinh(zm_1) \\ &+ R_n\cosh(zm_2) + S_n\sinh(zm_2),\end{aligned} \tag{21}$$

where the constants $P_n, Q_n, R_n, S_n$ are determined from the boundary conditions, Eqs. (8)–(10) and (13), and their values are given below.

By the substitution of Eq. (21) in Eq. (12), it can be deduced that $\widetilde{\zeta}_n$ satisfies

$$M_n\widetilde{\zeta}_n = a(\widetilde{\zeta}_{n-1} + \widetilde{\zeta}_{n+1}) \tag{22}$$

with

$$\begin{aligned}M_n &= \frac{2}{k}\left\{w_0^2 + \frac{m_1}{k}\left[\mu_n + k^2(3\nu_3 + \nu') - \nu_3 m_1^2\right]\frac{Q_n}{\widetilde{\zeta}_n}\right. \\ &\quad \left. + \frac{m_2}{k}\left[\mu_n + k^2(3\nu_3 + \nu') - \nu_3 m_2^2\right]\frac{S_n}{\widetilde{\zeta}_n}\right\} \\ &\equiv \frac{2}{k}D_n,\end{aligned} \tag{23}$$

and

$$w_0^2 := gk + \frac{\gamma k^3}{\rho}, \tag{24}$$

$$Q_n = \frac{\widetilde{\zeta}_n\mu_n A_1}{\left(m_1^2 - m_2^2\right)\left(1 + \frac{k^2\alpha}{\mu_n}\right) \times de},$$

$$\begin{aligned}A_1 = {}& -m_2\left(k^2 + m_1^2\right) - m_2\left[k^4\left(\frac{A}{\mu_n\eta_3}\frac{d\gamma}{dT} + 1\right) + k^2m_1^2\right]\frac{\alpha}{\mu_n} + \left\{k^2 + m_2^2 + \left[k^4\left(\frac{A}{\mu_n\eta_3}\frac{d\gamma}{dT} + 1\right) + k^2m_2^2\right]\frac{\alpha}{\mu_n}\right\} \\ &\times [m_2\cosh(Lm_1)\cosh(Lm_2) - m_1\sinh(Lm_1)\sinh(Lm_2)],\end{aligned}$$

$$S_n = \frac{\widetilde{\zeta}_n\mu_n B_1}{\left(m_1^2 - m_2^2\right)\left(1 + \frac{k^2\alpha}{\mu_n}\right) \times de},$$

$$de = -m_2\cosh(Lm_2)\sinh(\mathrm{Lm}_1) + m_1\cosh(Lm_1)\sinh(Lm_2),$$

$$B_1 = -m_1\left(k^2+m_2^2\right) - m_1\left[k^4\left(\frac{A}{\mu_n\eta_3}\frac{d\gamma}{dT}+1\right)+k^2m_2^2\right]\frac{\alpha}{\mu_n} + \left\{k^2+m_1^2+\left[k^4\left(\frac{A}{\mu_n\eta_3}\frac{d\gamma}{dT}+1\right)+k^2m_1^2\right]\frac{\alpha}{\mu_n}\right\}$$
$$\times\left[m_1\cosh(Lm_1)\cosh(Lm_2) - m_2\sinh(Lm_1)\sinh(Lm_2)\right],$$

$$P_n = -\frac{\widetilde{\zeta}_n\mu_n}{m_1^2-m_2^2}\left[k^2+m_2^2+k^4\frac{A}{\mu_n\eta_3}\frac{d\gamma}{dT}\frac{(\alpha/\mu_n)}{\left(1+k^2\frac{\alpha}{\mu_n}\right)}\right], \quad R_n = \frac{\widetilde{\zeta}_n\mu_n}{m_1^2-m_2^2}\left[k^2+m_1^2+k^4\frac{A}{\mu_n\eta_3}\frac{d\gamma}{dT}\frac{(\alpha/\mu_n)}{\left(1+k^2\frac{\alpha}{\mu_n}\right)}\right]. \quad (25)$$

Equation (22) provides the surface modes $\widetilde{\zeta}_n$ and depends on the Marangoni number $\mathrm{Ma} = (A/\mu_n\eta_3)d\gamma/dT$, thermal diffusivity $\alpha$, layer thickness $L$, the viscosities $\eta'$, $\eta_3$ and the known parameters $g$, $\gamma$, $\rho$ as well as on the given excitation frequency $\omega$ and shaker acceleration $a$. All of the material parameters of the fluid have been determined experimentally in Refs. [24,35]. In contrast for a system of semi-infinite thickness the following results are obtained:

$$M_n^{\infty} = \frac{2}{k}\left(w_0^2 - \frac{\mu_n}{k(m_1+m_2)\left(1+k^2\frac{\alpha}{\mu_n}\right)}\left\{[\mu_n+k^2(3\nu_3+\nu')](k^2-m_1m_2) - \nu_3k^2\left(m_1^2+m_2^2+m_1m_2\right) - \nu_3m_1^2m_2^2\right.\right.$$
$$\left.\left. + \frac{\alpha}{(m_1-m_2)^2}\left[A_2\left(m_1m_2+\nu_3m_1m_2^3+B_3m_2^2-\nu_3m_2^4\right)+B_2\left(m_1m_2+\nu_3m_1^3m_2+B_3m_1^2-\nu_3m_1^4\right)\right]\right\}\right)$$
$$\equiv \frac{2}{k}D_n^{\infty}(k,\mu_n = s+i(\alpha_r+n)w), \quad A_2 = k^4\left(\frac{A}{\mu_n\eta_3}\frac{d\gamma}{dT}+1\right)+k^2m_1^2, \quad B_2 = k^4\left(\frac{A}{\mu_n\eta_3}\frac{d\gamma}{dT}+1\right)+k^2m_2^2, \quad (26)$$

where $B_3 = \mu_n + (3\nu_3+\nu')k^2$.

### A. Critical parameters $a_c$, $k_c$ across the MBBA nematic-isotropic transition temperature

In this section we study the dispersion relation and acceleration of the surface modes across the nematic-isotropic transition. For the nematic phase of the liquid, we solved Eq. (22) with $s = 0$ to obtain the threshold of Faraday waves using standard numerical techniques of linear stability analysis [9,11]. The critical wave number $k_c$ and acceleration $a_c(k,\omega)$ versus temperature were obtained with $n = 22$. The light-scattering experiments of Langevin *et al.* [24] demonstrated that at the critical temperature $t_c \approx 45\,^{\circ}\mathrm{C}$ of MBBA, the anisotropy of the viscosities disappears and $\eta := \eta_3 = \eta_2, \eta' = 0$. Therefore, for the isotropic phase, we used hydrodynamic equations that are similar to those of a simple liquid and also coincide with the hydrodynamic equations of our second system obtained with an external magnetic field orthogonal to the wave vector direction, which is analyzed in Sec. III. Thus, the values of $a_c$ and $k_c$ where determined from Eq. (30) of Sec. III. Figure 1 depicts our main results for the transition experienced by dominant subharmonic waves of a MBBA (methoxy-benzilidine butyl aniline) liquid crystal from low temperatures in the nematic liquid phase $T - T_{\mathrm{NI}} < 0\,^{\circ}\mathrm{C}$ up to the high temperature range of the isotropic state $T - T_{\mathrm{NI}} > 0\,^{\circ}\mathrm{C}$ at two driving frequencies, the $\omega = 20\pi$ Hz open circles of Figs. 1(a) and 1(c) and the $\omega = 40$ Hz black circles and stars in Figs. 1(b) and 1(c), for layer thickness $L = 4.5$ mm. The circle symbols include the heat diffusivity $\alpha$ that produces Marangoni flow and was considered in the Marangoni number $(A/\mu_n\eta_3)d\gamma/dT$ in Eqs. (23)–(26). The star symbols neglect heat diffusivity and, thus, Marangoni flow. We observed that when Marangoni flow $\mathrm{Ma} = (A\mu_n\eta_3)d\gamma/dT$ is included, $a_c$ and $k_c$ roughly coincide with the values obtained when $\mathrm{Ma} = 0$ with as high as a 1% difference from each other. The same result is attained if the anisotropy of thermal diffusivity is taken either as $\alpha_{\parallel}$ or $\alpha_{\perp}$. Thus, in all our calculations we used only $\alpha_{\parallel}$ for the nematic side and $\alpha_{\mathrm{iso}}$ for the isotropic case.

Although a temperature gradient of $A = -3\,^{\circ}\mathrm{C/mm}$ acting vertically on MBBA produces noticeable changes in the

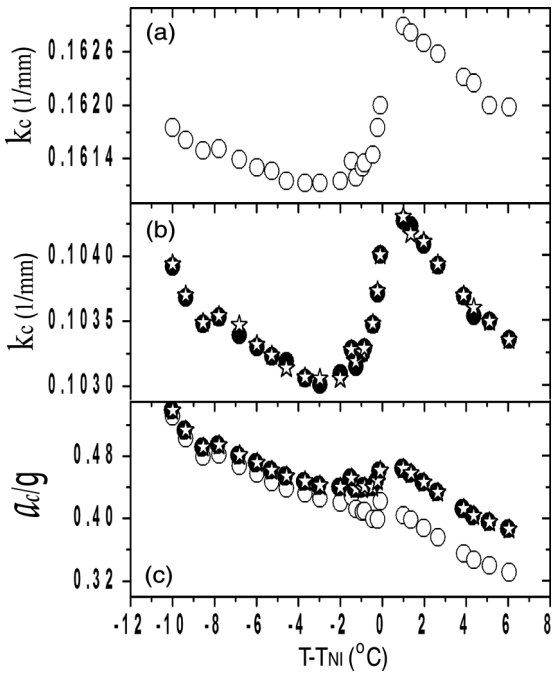


FIG. 1. Calculated critical parameters: $k_c$ (a, b) and $a_c$ (c) as a function of the nematic-isotropic transition temperature. External frequency $\omega = 20\pi$ Hz open circles (a, c), $\omega = 40$ Hz black dots and stars (b, c), and layer height $L = 4.5$ mm. Open and black circles include Marangoni flow, whereas it is neglected in the plot with star symbols. Viscosities and surface tension used were determined from Fig. 2.

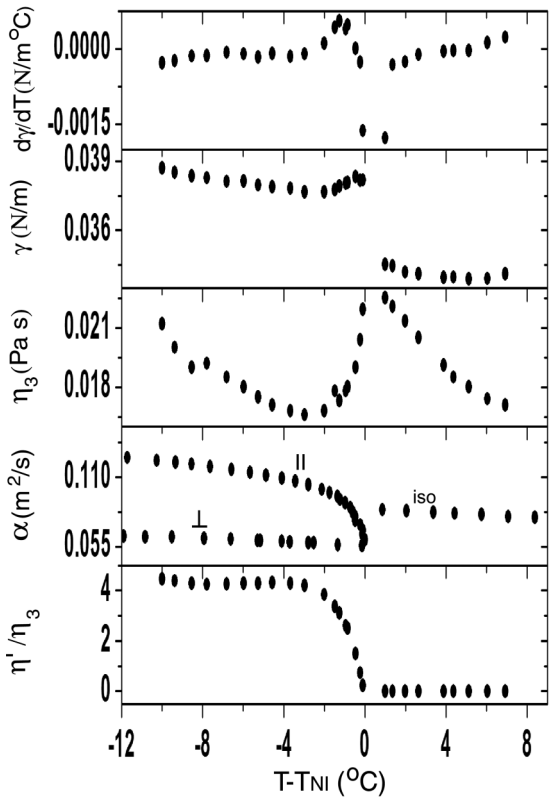


FIG. 2. Interpolated values of the gradient of surface tension with temperature $d\gamma/dT$, $\gamma$, viscosity $\eta_3$, thermal diffusivity $\alpha$, and viscosity $\eta'/\eta_3$ versus transition temperature. These values were obtained from the experimental data of Refs. [24,35] for MBBA.

viscosities and surface tension and thermal diffusivity (see Fig. 2), the gradient does not affect the Faraday waves. We can observe this phenomenon for $w = 40$ Hz in Fig. 1, where the Marangoni effect on $a_c$ and $k_c$, Figs. 1(b) and 1(c) (black circles) yields the same numerical values for these properties as in the case when Ma $= 0$ where Marangoni flow is neglected, results that can be seen in these same figures plotted with star symbols.

For these calculations, we used the experimentally measured temperature-dependent viscosities $\eta'(T - T_{\rm NI})$ and $\eta_3(T - T_{\rm NI})$ and the surface tension $\gamma(T - T_{\rm NI})$ reported in Refs. [24,27,35], and we assumed that the density $\rho = 1.03881 \times 10^3$ kg/m$^3$ was constant throughout the temperature interval, as required by the incompressibility condition Eq. (4); see Fig. 2. For the nematic side of this picture, we used Eq. (22). For the isotropic side, the analogous equation used was Eq. (30), which was derived as indicated in Sec. III. We also used the experimental values corresponding to $\eta_3(T - T_{\rm NI}) := \eta(T - T_{\rm NI})$ with $\gamma(T - T_{\rm NI})$ from Fig. 2 [24,35]. In the isotropic phase of the liquid, $a_c$ is increasing for the cooling process $T - T_{\rm NI} < 7\,^\circ$C [see Fig. 1(c)] with a drop of $\sim$0.25 $g$ at the transition $T_c = 45\,^\circ$C, and the value keeps increasing in the nematic phase for $T - T_{\rm NI} < 0\,^\circ$C. In general, the observed drop in $a_c$ is only a fraction of $g$. For instance, the open circle symbols refer to this same property calculated at the high frequency $w = 40\pi$ Hz and displays the same magnitude for the variation of the acceleration at the transition temperature as for the lower frequency case. In contrast, $k_c$ similarly exhibits an increasing trend with a small drop of 0.0013 mm$^{-1}$ or 1.0 mm in wavelength through the transition temperature [Fig. 1(b)] and still exhibits a much smaller decrease for the smaller frequency $w = 20\pi$ Hz case, where it is only half of a millimeter in wavelength; see Fig. 1(a). These discontinuous changes of both properties are in accordance with similar discontinuous behaviors displayed by the large temperature variations experienced by the viscosities $\eta'$, $\eta_3$ and surface tension in the experimental data. The discontinuity in $a_c$ and $k_c$ versus temperature observed here is due to viscosities and surface tension changes due to Marangoni flow affecting those material parameters. A different mechanism for discontinuities in these critical parameters appeared during the surface freezing of a tetracosanol melt, as documented in the experiments of Huber *et al.* [36,37]. In their system, decreasing the temperature led to the formation of a surfactant interfacial monolayer that changes the surface tension, with a negligible change of bulk viscosity, resulting in a high flow velocity gradient close to the surface at a given temperature during the cooling down process from the high-temperature regime of the melt. Unlike the MBBA liquid where the director **n** is kept oriented by the field $H$, the exact match of the experimentally measured power spectrums of scattered light by thermal fluctuations of the nematic-air interface with those of a theoretical calculation ignoring Marangoni flow at a fixed temperature suggest that a monolayer of nematogens does not form at the interface [38]. However, the critical parameters of the Faraday instability for the liquid-vapor interface of $CO_2$ [9,39] do not present such discontinuities as we observed here for the MBBA liquid.

The neutral stability curve $a(k,\omega)$ versus wave number $k$, was obtained (see Fig. 3) using a model nematic system with parameters $\eta' = 4.26\eta_3$, a higher viscosity by a factor of 10 $\eta_3 = 0.163$ Pa s with respect to the experimental data of [38] for MBBA, $\gamma = 0.03853$ N/m and $\rho = 1.03881 \times 10^3$ kg/m$^3$. The magnetic induction was $|\mathbf{B}| = 0.3$ T and the constant temperature was $T_{\rm NI} - T = 3\,^\circ$C from the nematic-isotropic transition. Figures 3(a)–3(c) demonstrate the effect on the instability "tongues" due to an increase of frequency $\omega$ for the fixed layer thickness $L = 2$ mm in all the cases. The main mode is subharmonic (filled circle). When the frequency increases, the number of tongues diminishes and become enhanced, thus covering wider wave numbers intervals. In addition, a secondary harmonic mode becomes the critical instability at $\omega \approx 120\pi$ Hz (open circle), dominating the other mode type from them on. Such a change of wave mode occurs at the bicritical instability $a_c \approx 33$ $g$, which corresponds to wave numbers $k_c \approx 0.856$, and 1.674 mm$^{-1}$; see Table I. From this table we note that the model nematic has a bicritical acceleration and wave number on the same order of magnitude as for a concentrated polymer solution of a single relaxation time [19]. A second bicritical instability is reached at $\omega = 1265$ Hz.

The first bicritical instability can be avoided by making the sample of nematic liquid thicker in the container, for instance, to $L = 2.5$ mm. This increase in the depth of liquid produces again dominant subharmonic critical behavior [Fig. 3(d)]. Figure 4 presents the dispersion relation of the real MBBA [inset of Fig. 4(a)] and of the model nematic referred to

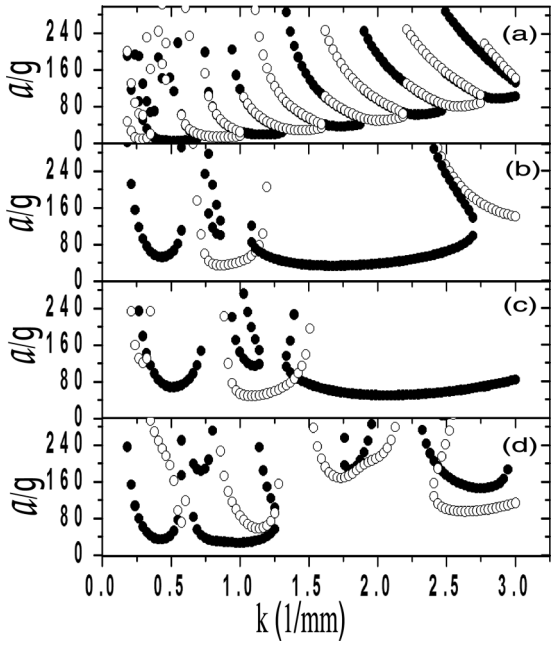


FIG. 3. Neutral stability curves of a model nematic liquid crystal with Ma = 0. A static magnetic field is applied parallel to the wave vector **k** and to the equilibrium liquid interface, with magnetic induction $|\mathbf{B}| = 0.3$ T, and temperature $T_{NI} - T = 3\,^{\circ}$C from the nematic-isotropic transition. Layer thickness $L = 2$ mm and external frequencies in panels (a) $\omega = 20\pi$ Hz, (b) $\omega = 120\pi$ Hz, (c) $\omega = 160\pi$ Hz, (d) $\omega = 160\pi$ Hz for $L = 2.5$ mm. Other system's parameters are given in Sec. II A. • subharmonic mode, ○ harmonic.

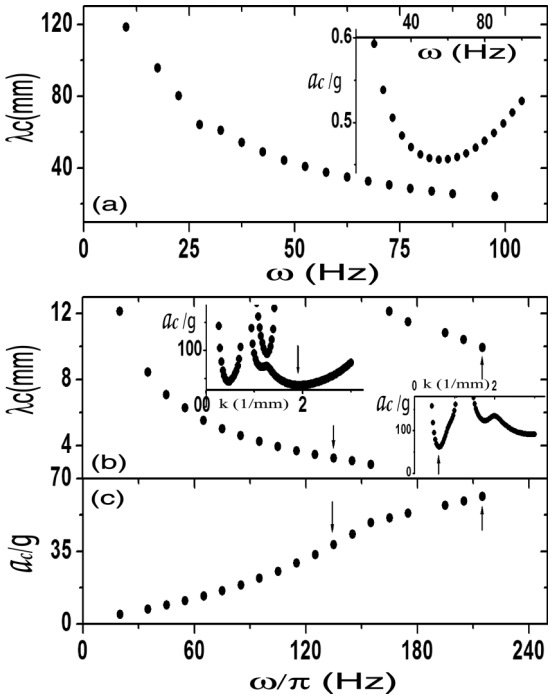


FIG. 4. Subharmonic's dispersion relation of nematic liquid with depth $L = 4.5$ mm (a) and 2.5 mm (b, c). Inset of panel (a) depicts the critical acceleration with Marangoni number calculated with real material properties interpolated from Fig. 2. Panels (b) and (c) correspond to a model nematic with 10 times viscosity in (a) and neglects Marangoni flow. Its critical acceleration is given in (c). Left (with down arrow ↓) and right (with up arrow ↑) insets depict critical accelerations $a_c/g = 38.15$, 51.13 occurring at $k_c = 1.9284$ and 0.6312 mm$^{-1}$ and $\omega = 135\pi$ and $215\pi$ Hz, respectively.

above [Figs. 4(b) and 4(c)]. The real MBBA liquid [Fig. 4(a)] has a minimum at $a_c \approx 0.4554\ g$ for $\omega = 55$ Hz and $L = 4.5$ mm with the Marangoni number $\mathrm{Ma} = (A/\mu_n\eta_3)d\gamma/dT$ considered, whereas the model nematic with the higher bulk viscosity $\eta_3 = 0.163$ Pa s and $L = 2.5$ mm, with Ma = 0, presents a monotonously increasing $a_c$ [Figs. 4(b) and 4(c)]. Müller *et al.* also observed a minimum in $a_c$ in silicon oil and water systems, where they incorporated the dissipation of boundary layers along the container walls and beneath the surface into their analytical description of

TABLE I. A nematic system with $L = 2$ mm.

| $\omega/\pi$ (Hz) | Mode | $a_c/g$ | $k$ (mm$^{-1}$) |
|---|---|---|---|
| 20 | Har | 9.12 | 0.2928 |
| | Sup | 6.13 | 0.5184 |
| 40 | Har | 13.04 | 0.4056 |
| | Sub | 10.52 | 0.8286 |
| 80 | Har | 21.95 | 0.6594 |
| | Sub | 20.35 | 1.2798 |
| 100 | Har | 27.22 | 0.7440 |
| | Sub | 26.31 | 1.4772 |
| 120 bicritical | Har | 33.08 | 0.8568 |
| | Sub | 33.17 | 1.6746 |
| 160 | Har | 47.12 | 1.0822 |
| | Sub | 50.14 | 2.0694 |

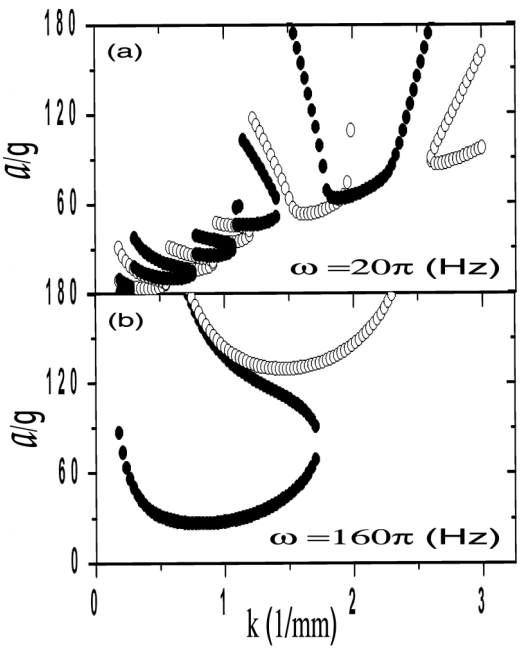


FIG. 5. Faraday thresholds of model semi-infinite limit system without Marangoni flow (symbol • subharmonic mode and ○ is harmonic one). Same fluid parameters as in Fig. 3.

their experiments [10]. However, our second model system so defined has a discontinuous dispersion relationship, as can be observed in Fig. 4(b). In this figure the critical wavelength $\lambda_c$ of the subharmonic wave versus $\omega$ decreases continuously. At the frequency $\omega/2\pi \approx 165\pi$ Hz, this wavelength has changed sharply to the same starting value $\lambda_c = 12.1203$ mm it had at the beginning of the stimulus excitation $\omega \approx 20\pi$ Hz. The insets of Fig. 4(b) show the transition from the main subharmonic wave (down arrow for $k_c = 1.9284$ mm$^{-1}$) to a secondary one (up arrow for $k_c = 0.6312$ mm$^{-1}$ in this example); it becomes the main subharmonic instability at $\omega \approx 215\pi$ Hz. Figure 4(c) depicts the critical acceleration $a_c$ as a continuously increasing function of $\omega$. A change of slope is observed at $k_c = 0.5184$ mm$^{-1}$, corresponding to the change in wavelength as described in Fig. 4(b). A similar transition from a subharmonic to harmonic response with wavelength discontinuity has been described in Refs. [16,19,40] for the interface of viscoelastic fluids, Ref. [11] for Newtonian fluid, and Ref. [10] for silicon oil and water systems.

For half-infinite systems, Eq. (22) is now solved numerically using Eq. (26) when Ma $= 0$ and $\alpha = 0$ m$^2$/s. We see in Fig. 5 that surface Faraday waves are also sustained in the semi-infinite medium of nematic liquids. The critical acceleration to obtain these modes is on the order of tenths of $g$ and always corresponds to the subharmonic type. When the frequency is increased the instability boundaries experiences a shift to amplify its interval of $a/g$ as a function of wave numbers values, as demonstrated in Figs. 5(a)–5(b).

### B. Thermal waves

We note that for $a = 0$, $s = 0$, $\alpha_r = 0$, and $n = 0$, $D_n(k,\mu_n = iw) = 0$ is the dispersion relation of a finite thickness layer experiencing thermal surface waves with Marangoni flow. Such a dispersion relationship has not been reported before in the literature. However, its semi-infinite medium version $L \to \infty$ given by $D^{\infty}_{n=0}(k,\mu_n = iw) = 0$ [Eq. (26)] coincides with the one reported in Refs. [24,27] after using for $m_1 m_2 := \epsilon k^2\sqrt{(1+2S_L)}$, $m_1^2 + m_2^2 := \mu_n/\nu_3 + k^2(2+\nu'/\nu_3)$ with $S_L := iw/2\nu_3 k^2$ and $\epsilon = +1$ if $\nu'/\nu_3 > -2$, and for Ma $= 0$, with no thermal diffusion $\alpha = 0$ m$^2$/ s.

It was demonstrated by Ballesta *et al.* [20] that in their lyotropic liquid crystal, the external parametric excitation generated an oscillatory shear of strain on the order of 260 s$^{-1}$ beneath the surface pattern. Such a high amplitude of shear rate formed transient patches of local nematic ordering in the wave's crest. If there is no magnetic field fixing the orientation of the nematic director as in our systems here, then the director may experience spatial variations due to the generated stress.A calculation performed by Burghardt [41] demonstrated that a nematic liquid subjected to oscillatory shear flow exhibits viscoelastic character. Therefore, an experiment such as the one performed by Ballesta *et al.* might be useful to study the interfacial rheology of the director rotation with the induced stress for a given set of driving acceleration and frequency. However, in this case, our expression for the fluid inertial effect accounted for through Eq. (2) would need to be modified to include the coupling of the balance of torque of the director due to the elastic distortion of the nematic layers that produce a viscous response of the liquid crystal.

## III. MAGNETIC FIELD PARALLEL TO THE *Y* AXIS, AND WAVE VECTOR DIRECTED ALONG THE *X* AXIS

In this case the director is defined by $\mathbf{n} = (0,1,0)$ and is perpendicular to the velocity field $\mathbf{v}$, $\mathbf{n}\perp\mathbf{k}$. Therefore, there is no hydrodynamic coupling between the director and flux, and the hydrodynamic equations are of an isotropic fluid with one viscosity $\eta :\equiv \eta_3 = \eta_2$. Thus, from Eq. (1) the stress tensor components are [24,27]

$$\boldsymbol{\sigma}'_{xx} = 2\eta\partial_x v_x, \quad \boldsymbol{\sigma}'_{zz} = 2\eta\partial_z v_z, \quad \boldsymbol{\sigma}'_{zx} = \eta(\partial_x v_z + \partial_z v_x). \tag{27}$$

The capillary force at the interface becomes

$$\sigma^r_{zz} = f_z = \gamma\left(\partial_x^2 + \partial_y^2\right)\zeta(x), \tag{28}$$

with the presence of tangential forces given by [30]

$$\begin{aligned} \sigma^r_{xz} &= f_x = \frac{d\gamma}{dT}[\partial_x T - A\partial_x\zeta(x)], \\ \sigma^r_{yz} &= f_y = 0. \end{aligned} \tag{29}$$

The boundary conditions are as reported in Sec. II, and the diffusion equation (3) is satisfied. The procedure to obtain the instability modes $\widetilde{\zeta}_n$ follows the methods used to derive Eq. (22) as described in the previous section. Here, however, the resulting equation is identical to that of an isotropic Newtonian fluid characterized by one viscosity, and surface tension [9,11] and Marangoni number Ma $= (A/\mu_n\eta)d\gamma/dT$. The result is

$$M^i_n\widetilde{\zeta}_n = a(\widetilde{\zeta}_{n-1} + \widetilde{\zeta}_{n+1}), \tag{30}$$

with

$$M^i_n = \frac{2}{k}\left\{w_0^2 + \nu\left(q_n^2 + k^2\right)\frac{Q^i_n}{\widetilde{\zeta}_n}\right\} + 4\nu q_n\frac{S^i_n}{\widetilde{\zeta}_n}, \tag{31}$$

where

$$\begin{aligned} Q^i_n = \widetilde{\zeta}_n\Bigg(&\nu q_n k^2\Bigg\{-2\left(1+k^2\frac{\alpha}{\mu_n}\right) + \frac{A}{\nu\eta}\frac{d\gamma}{dT}\frac{1}{k^2-q_n^2}\left[1 - q_n^2\frac{\nu}{\mu_n} + (\nu+\alpha)\frac{k^2}{\mu_n}\right]\Bigg\} + \nu\Bigg\{-\left(k^2+q_n^2\right)\left(1+k^2\frac{\alpha}{\mu_n}\right) \\ &+ \frac{A}{\nu\eta}\frac{d\gamma}{dT}\frac{k^2}{k^2-q_n^2}\left[1 - q_n^2\frac{\nu}{\mu_n} + (\nu+\alpha)\frac{k^2}{\mu_n}\right]\Bigg)[-q_n\cosh(kL)\cosh(q_nL) + k\sinh(kL)\sinh(q_nL)]\Bigg\} \\ &\Big/\left\{\left(1+k^2\frac{\alpha}{\mu_n}\right)[q_n\cosh(q_nL)\sinh(kL) - k\cosh(kL)\sinh(q_nL)]\right\}, \end{aligned}$$

$$S_n^i = \tilde{\zeta}_n \nu k \Big\{ k^2 + q_n^2 - 2k[k\cosh(kL)\cosh(q_nL) - q_n\sinh(kL)\sinh(q_nL)] - k^2 \frac{A}{\nu\eta}\frac{d\gamma}{dT}\left(\frac{1}{k^2-q_n^2} + \frac{\nu}{\mu_n + k^2\alpha}\right) + k\frac{A}{\nu\eta}\frac{d\gamma}{dT}\left(\frac{1}{k^2-q_n^2} + \frac{\nu}{\mu_n + k^2\alpha}\right)[k\cosh(kL)\cosh(q_nL) - q_n\sinh(kL)\sinh(q_nL)]\Big\} \times [-q_n\cosh(q_nL)\sinh(kL) + k\cosh(kL)\sinh(q_nL)]^{-1}, \quad (32)$$

with $\nu = \eta/\rho$ and $q_n^2 := \mu_n/\nu + k^2$. We studied two systems: the real MBBA with materials parameters for surface tension $\gamma = 0.03803$ N/m, density $\rho = 1.03854 \times 10^3$ kg/m$^3$, and viscosity $\eta = 0.0252$ Pa s, as given in Ref. [38]. The applied magnetic induction is $|\mathbf{B}| = 0.3$ T and temperature $T - T_{\rm NI} = 3$ °C from the nematic-isotropic transition Ref. [38], and a model nematic liquid with the same parameters but with 10 times higher dynamical viscosity $\eta = 0.252$ Pa s.

The neutral stability curve as a function of wave number for the second model system is given in Fig. 6. In this figure we can observe both the effect of increasing the thickness of the layer [Figs. 6(a) and 6(b)] and of increasing the frequency [Figs. 6(c) and 6(d)]. In addition, one can observe that the main critical instability is of subharmonic nature (the filled circle symbol represents a subharmonic mode and the open circle symbol represents a harmonic mode). Unlike for the previous case, $\mathbf{n}\|\mathbf{v}$, there is no bicritical instability. These plots demonstrate that the curves $a(k,\omega)$ versus $k$ of a finite depth layer system exhibit the same qualitative behavior as the semi-infinite medium case of the previous section when $\mathbf{n}\|\mathbf{k}$. For instance, from Fig. 6(b) and for increasing $\omega$, we find that the values of $a/g$ are of approximately the same order of magnitude as those in Fig. 5(a) for the case $\mathbf{n}\|\mathbf{k}$. Figure 7 presents two useful properties, the dispersion relation and critical acceleration curves, for two systems: one has thickness $L = 4.5$ mm [Fig. 7(a) and includes Marangoni flow, and the second one for $L = 2.5$ mm with Ma $= 0$ is depicted in Fig. 7(b). These properties should be helpful in estimating the values of $\gamma$ and $\eta$ from a comparison with experimental data on nematics. Figures 8(a) and 8(b) present the stability phase diagrams of a semi-infinite medium for the second model system with Ma $= 0$, which we observe do not differ quantitatively much from the finite depth cases of Figs. 6.

Finally, Figure 8(c) confirms our previous observation that the limit $L \to \infty$ systems, when the director is either parallel or perpendicular to the flow, roughly coincides quantitatively for $k \lessapprox 1.5$ mm$^{-1}$ and start to disagree only at higher wave numbers and frequencies.

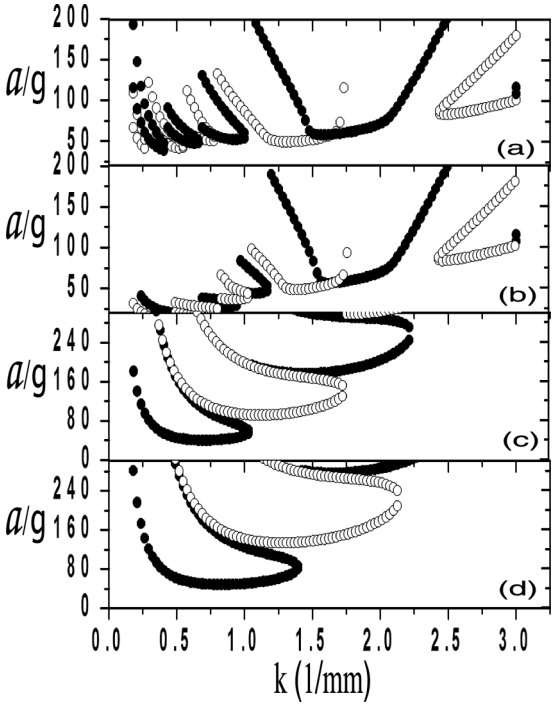


FIG. 6. Instability threshold of model nematic liquid with order parameter perpendicular to wave vector, with magnetic induction $|\mathbf{B}| = 0.3$ T, Ma $= 0$, $\alpha = 0$ m$^2$/s, and temperature $T - T_{\rm NI} = 3$ °C from the nematic-isotropic transition. Modulation frequency and depth of material for (a) $\omega = 20\pi$ Hz, $L = 2$ mm, (b) $\omega = 20\pi$ Hz, $L = 6$ mm, (c) $\omega = 120\pi$ Hz, $L = 2$ mm, and (d) $\omega = 160\pi$ Hz, $L = 2$ mm. Other parameters are given in Sec. III (• subharmonic mode and ○ harmonic wave).

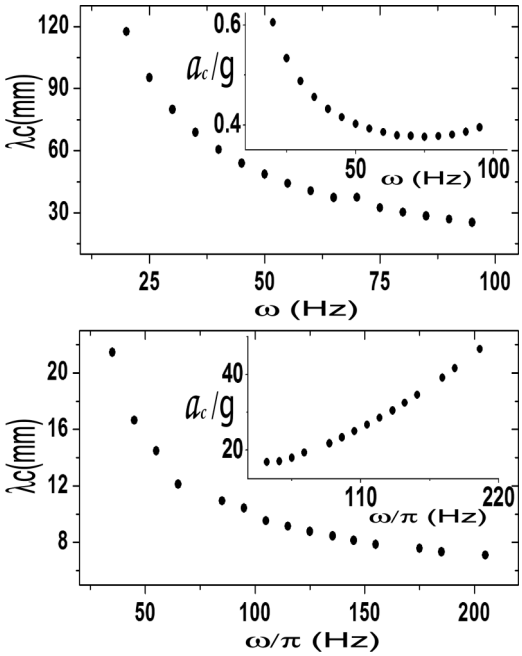


FIG. 7. Dispersion relation of critical subharmonic threshold for depth $L = 4.5$ (a) and 2.5 mm (b). Panel (a) was calculated using the real materials data and taking the corresponding Marangoni number, whereas panel (b) is for a model nematic with 10 times the viscosity of (a) and zero Marangoni number. Inset depicts the critical acceleration versus excitation frequency. Other parameters are given in Sec. III.

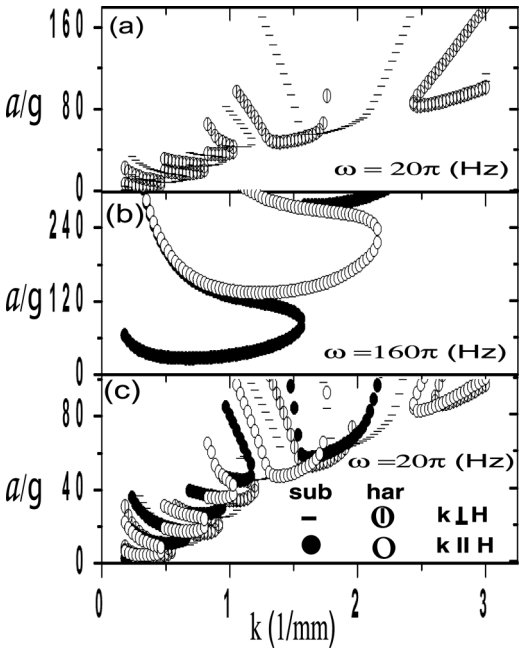


FIG. 8. Accessible surface modes given by the stability curves $a/g$ as a function of wave number $k$. Semi-infinite medium of nematic liquid. The material properties are given in Sec. III. Panel (c) is a superposition of panel (a) and Fig. 5(a), and they depict the quantitative coincidence of the first boundaries for low wave vectors.

## IV. CONCLUSIONS

In this paper, we presented a description of the instability curve and dispersion relation for nematic liquid crystals under a static magnetic field orienting the nematogens parallel to the equilibrium liquid-air interface and under a temperature gradient. We observed that the critical parameters $a_c$, $k_c$ of a standing instability pattern are discontinuous for MBBA at the nematic-isotropic transition temperature for layers with thicknesses of a few millimeters. High-velocity gradients set in near the surface due to the underlying large temperature variation that experience the bulk viscosities $\eta'$, $\eta_3$ and surface tension due to Marangoni flow.

For realistic and model nematics with higher viscosity compared with real MBBA, we analyzed the dispersion relations along the nematic-isotropic transition of a nematic liquid crystal. We used parameters of a typical nematic. In realistic MBBA, for layers of depth $L = 4.5$ mm, the critical acceleration exhibits a minimum with $\mathrm{Ma} \neq 0$ whereas the higher viscous model with $L \leqslant 2$ mm, $\mathrm{Ma} = 0$, is monotonously increasing. For hydrodynamic coupling of the director $\mathbf{n}$ with the wave vector flow $\mathbf{k}$, $\mathbf{n} \| \mathbf{k}$ case, a linear stability analysis reveals a bicritical instability for the second model nematic about $a_c/g \approx 33$ with critical wave numbers $k_c \approx 0.8568$ and $1.6746\ \mathrm{mm}^{-1}$. Here a crossover occurs from the critical subharmonic mode into the harmonic type when the frequency reaches the value $\omega \approx 120\pi$ Hz (Table I). The bicritical instability can be avoided when the layer thickness is increased to as high as 2.5 mm, where the system is observed to sustain only critical waves of the subharmonic type. However, the dispersion relation of these waves [Fig. 4(b)] develops a discontinuous shift of the critical wavelength as a function of frequency near $\omega \approx 165\pi$ Hz, where a secondary instability of lower wave number becomes dominant. When the layer thickness reaches its semi-infinite limit ($L \to \infty$), the critical instability zones are always subharmonic and become enhanced when the frequency is increased. For values $a/g = 0$, we obtained a new dispersion relationship of thermal surface waves on a finite thickness of nematic liquids layers under Marangoni flow. When there is no hydrodynamic coupling of the director with the flow, $\mathbf{n} \perp \mathbf{k}$, the Navier-Stokes equation of an isotropic liquid characterized by surface tension $\gamma$ and a single viscosity $\eta$ as the only material parameters is satisfied. Both for the finite layer and semi-infinite system, their stability boundaries ($a/g$ vs $k$ curve) exhibit the same general trends as for the $\mathbf{n} \| \mathbf{k}$ case above. Furthermore, in both cases, they coincide quantitatively for low wave numbers $k \lessapprox 1.5\ \mathrm{mm}^{-1}$ and begin to disagree at higher wave numbers and frequencies [see Fig. 8(c)] when Marangoni flow is neglected.

## ACKNOWLEDGMENTS

The author acknowledges the General Coordination of Information and Communications Technologies (CGSTIC) at CINVESTAV for providing HPC resources on the Hybrid Supercomputer "Xiuhcoatl", which has contributed to the research results reported within this paper. We would like to thank the referees for their very useful comments and criticisms. This work was supported by CONACYT Grant No. 48794-F, Mexico.

[1] A. C. Skeldon and G. Guidoboni, SIAM J. Appl. Math. **67**, 1064 (2007).
[2] W. S. Edwards and S. Fauve, J. Fluid Mech. **278**, 123 (1994).
[3] J. Bechhoefer, V. Ego, S. Manneville, and B. Johnson, J. Fluid Mech. **288**, 325 (1995).
[4] E. Cerda and E. Tirapegui, Phys. Rev. Lett. **78**, 859 (1997).
[5] P. Chen and J. Vinals, Phys. Rev. Lett. **79**, 2670 (1997).
[6] O. Lioubashevski, Y. Hamiel, A. Agnon, Z. Reches, and J. Fineberg, Phys. Rev. Lett. **83**, 3190 (1999).
[7] P. Engels, C. Atherton, and M. A. Hoefer, Phys. Rev. Lett. **98**, 095301 (2007).
[8] P. Capuzzi and P. Vignolo, Phys. Rev. A **78**, 043613 (2008).
[9] K. Kumar and L. S. Tuckerman, J. Fluid Mech. **279**, 49 (1994).
[10] H. W. Müller, H. Wittmer, C. Wagner, J. Albers, and K. Knorr, Phys. Rev. Lett. **78**, 2357 (1997).
[11] K. Kumar, Proc. R. Soc. Lond. A **452**, 1113 (1996).
[12] S. Douady, J. Fluid Mech. **221**, 383 (1990).
[13] H. W. Müller, Phys. Rev. Lett. **71**, 3287 (1993).
[14] V. V. Mekhonoshin and A. Lange, Phys. Rev. E **65**, 061509 (2002).
[15] T. Mahr and I. Rehberg, Phys. Rev. Lett. **81**, 89 (1998).
[16] H. W. Müller and W. Zimmermann, Europhys. Lett. **45**, 169 (1999).

[17] C. Wagner, H. W. Müller, and K. Knorr, Phys. Rev. Lett. **83**, 308 (1999).
[18] F. Raynal, S. Kumar, and S. Fauve, Eur. Phys. J. B **9**, 175 (1999).
[19] S. Kumar, Phys. Fluids **11**, 1970 (1999).
[20] P. Ballesta and S. Manneville, Phys. Rev. E **71**, 026308 (2005).
[21] T. Epstein and R. D. Deegan, Phys. Rev. E **81**, 066310 (2010).
[22] P. Ballesta, M. P. Lettinga, and S. Manneville, Soft Matter **7**, 11440 (2011).
[23] N. Périnet, D. Juric, and L. S. Tuckerman, J. Fluid. Mech. **635**, 1 (2009).
[24] D. Langevin and M. A. Bouchiat, J. Physique **33**, 101 (1972).
[25] P. G. de Gennes and J. Prost, *The Physics of Liquid Crystals* (Clarendon, Oxford, 1993).
[26] A. Buka and W. H. de Jeu, J. Physique **43**, 361 (1982).
[27] D. Langevin, *Scattering by Liquid Surfaces and Complementary Techniques* (Dekker, New York, 1992).
[28] D. Langevin and M. A. Bouchiat, Mol. Cryst. Liq. Cryst. **22**, 317 (1973).
[29] P. C. Martin, O. Parodi, and P. S. Persham, Phys. Rev. A **6**, 2401 (1972).
[30] R. V. Birikh, V. A. Briskman, A. A. Cherepanov, and M. G. Velarde, J. Colloid. Interf. Sci. **238**, 16 (2001).
[31] M. A. Vila, V. A. Kuz, A. N. Garazo, and A. E. Rodriguez, J. Physique **48**, 1895 (1987).
[32] C. H. Wang and Q. R. Huang, J. Chem. Phys. **107**, 5898 (1997).
[33] F. Monroy, F. Ortega, and R. G. Rubio, Phys. Rev. E **58**, 7629 (1998).
[34] M. Hernández-Contreras, J. Phys.: Condens. Matter **22**, 035106 (2010).
[35] W. Urbach, H. Hervet, and F. Rondelez, Mol. Cryst. Liq. Crystl. **46**, 209 (1978).
[36] P. Huber, V. P. Soprunyuk, J. P. Embs, C. Wagner, M. Deutsch, and S. Kumar, Phys. Rev. Lett. **94**, 184504 (2005).
[37] S. Kumar and O. K. Matar, Phys. Fluids **16**, 39 (2004).
[38] D. Langevin, J. Physique **33**, 249 (1972).
[39] S. Fauve, K. Kumar, C. Laroche, D. Beysens, and Y. Garrabos, Phys. Rev. Lett. **68**, 3160 (1992).
[40] S. Kumar, Phys. Rev. E **65**, 026305 (2002).
[41] W. R. Burghardt, J. Rheol. **35**, 49 (1991).